Femtosecond pump–probe study of preformed plasma channels

Rafal Zgadzaj, Erhard W. Gaul, Nicholas H. Matlis, Gennady Shvets, and Michael C. Downer

FOCUS Center, University of Texas at Austin, Department of Physics, Austin, Texas 78712-1081

Received November 8, 2003; revised manuscript received March 23, 2004; accepted March 31, 2004

We report femtosecond pump–probe experiments in He plasma waveguides using 800-nm, 80-fs pump pulses of 0.2×10^{18} W/cm^2 peak guided intensity and single orthogonally polarized 800-nm probe pulses ~0.1% as intense as the pump. Single-shot spectra and spatial profiles of the probe pulses exiting the channels are measured through a crossed-polarization analyzer at various pump–probe time delays Δt. At $|\Delta t| \gtrsim 100$ fs, we observe frequency-domain interference between the probe and a weak component of the exiting pump created by hybridization of its polarization state through interaction with the channel. Frequency-domain interference measurements show this "depolarized" component differs substantially in mode structure from the injected pump pulse. This component is nearly undetectable by direct measurements of pump leakage without the probe. We analyze possible causes of depolarization within the channel and near its entrance and exit regions. At $\Delta t \leq 0$, i.e., the probe pulse propagates in the leading edge of the pump pulse, we observe spectral blueshifts in the transmitted-probe spectrum that are not evident in the transmitted pump. The evidence indicates that pump depolarization and probe blueshifts both originate primarily near the channel entrance.

OCIS codes: 320.0320, 230.7380, 350.5400, 320.7100.

1. INTRODUCTION

Preformed plasma waveguides capable of controllably guiding relativistically intense femtosecond (fs) laser pulses over multiple Rayleigh lengths (z_R) without optical distortion are essential to developing GeV-scale laser-wakefield accelerators and coherent short-wavelength sources.[1] *Single* pulses with peak intensity as high as ~10^{17} W/cm^2 have been guided through plasma channels generated by two main methods.[2–9] One type of channel is formed inside solid capillaries (e.g., by ablating the inner wall[2,3] or by thermally inducing density gradients in a hydrogen-filled interior[5]). Such channels tend to support modes with radii in the range $20 < w_0 < 40\ \mu$m, are usually limited to low repetition rates (<1 Hz), and require parts that must be replaced after a finite number of shots. A second type of channel, developed by Milchberg and coworkers,[6] is formed by cylindrical shock waves emanating from the line focus of a laser in a gas backfill[6,7] or jet.[8,9] These channels tend to support smaller modes ($w_0 < 10\ \mu$m), can operate at higher repetition rates (≲20 Hz), and are indefinitely replenishable. We recently reported distortion-free guiding of *single* 80-fs pulses over $60 z_R$ (1.5 cm) at $I_{\text{guided}} \approx 2 \times 10^{17}$ W/cm^2 in a fully ionized channel of this second type formed in a He backfill.[7]

In this paper, we extend the previous study by reporting fs pump–probe experiments with pump intensity $I_{\text{guided}} \approx 2 \times 10^{17}$ W/cm^2 in the fully ionized He channel. Just as *un*channeled pump–probe experiments have proven to be essential in elucidating the fs dynamics of many high-field phenomena (e.g., ionization,[10] solid surface,[11,12] and cluster[13] expansion and plasma wakefields[14–18]), *channeled* pump–probe techniques promise to enable the characterization of plasma dynamics within channels, both during and after the passage of the main pulse. In particular, double-probe frequency-domain interferometry (FDI), which has come into widespread use in high-field laser-plasma experiments[11–15,18] is well suited for plasma channel diagnostics because of its high sensitivity and its ability to yield fs-time- and μm-space-resolved data in both multishot[14,15,18] and single-shot[19,20] configurations. In the present study, FDI was used to characterize the spectral structure of an exiting guided probe pulse or the spatial mode of a depolarized component of a guided pump pulse in a single shot.

To extend FDI to plasma channels, however, several new factors must be considered. First, the interaction length inside the channel is long enough ($L \geq 1$ cm) that group-velocity walk-off between the pump and probe pulses becomes important when the wavelengths differ significantly ($\Delta\lambda \equiv \lambda_{\text{probe}} - \lambda_{\text{pump}} \neq 0$). While the traditional use of different wavelengths is an effective method to enhance discrimination of probe from scattered pump light, pump–probe walk-off degrades time resolution and thus severely restricts the useful range of $\Delta\lambda$. As an example, to probe wake oscillations at axial densities $n_e(r = 0) \geq 5 \times 10^{18}$ cm^{-3} typical of Milchberg-type channels, pump–probe walk-off should be $\leq \lambda_p/4$ to avoid washing out the wave structure, necessitating $\Delta\lambda \leq \lambda_p^3/4L\lambda_{\text{pump}} \approx 0.07\ \mu$m for $L = 1.5$ cm, $\lambda_{\text{pump}} = 0.80\ \mu$m. Second-harmonic[15,19] or white-light continuum[13] probes used in previous FDI experiments are therefore no longer useful. For practical purposes, $\lambda_{\text{probe}} = \lambda_{\text{pump}}$ is required. Consequently, in the present work, we employ orthogonally polarized pump and probe pulses of equal wavelength $\lambda_{\text{probe}} = \lambda_{\text{pump}} = 800$ nm, and we use polarization discrimination to isolate the probe at the detector.

Second, coupling one pulse efficiently into the small entrance of Milchberg-type channels is already difficult. Coupling 2 (or more) probes as required for FDI compounds the difficulty. In this work we show that, for pump–probe time delays Δt larger than the inverse pulse bandwidth $2\pi/\Delta\omega$ (~100 fs for our conditions), channeled FDI can be implemented using only a *single* externally injected probe pulse, while using a depolarized component of the pump pulse as a second "built-in" reference pulse at the same λ. This component can be created intentionally by rotating the incident pump polarization, or advantage can be taken of the natural pump depolarization inherent in its interaction with the channel. Although the former procedure may be preferred for many experiments, in this paper we focus on the latter case because of the importance of characterizing and understanding the depolarized light as an unavoidable background in pump–probe experiments and as a diagnostic of the channel and its entrance/exit regions.

Third, cumulative frequency shifts $\Delta\lambda_{\text{probe}}$ of the trailing probe caused by ionization[10] or photon acceleration[21] in a plasma wake can become sizeable over a ≥1-cm channel. If $\Delta\lambda_{\text{probe}}$ approaches or exceeds the reference-pulse bandwidth, interpretation of FDI data is significantly affected.[22] Moreover, direct measurement of $\Delta\lambda_{\text{probe}}$ can become the preferred diagnostic. Our current experiments illustrate the use of ionization-induced blueshifts $\Delta\lambda_{\text{probe}}$ to complement FDI as a diagnostic of probe-pulse propagation through a channel at small Δt, where FDI fringes are too widely separated to be useful.

2. EXPERIMENTAL SETUP

Our procedure for generating, characterizing, and guiding intense fs laser pulses through fully ionized He channels has been described previously.[7] Channels are created by sending 400-ps, 1-J Nd:YAG laser pulses through an axicon lens into a 400-Torr He backfill. The resulting 1-cm-long line focus ionizes and heats the gas, driving a cylindrical shock wave radially outward. Figure 1(a) summarizes our diagnostic measurements of the channels and guided pump pulses used for the present pump–probe experiments. The top row shows the expanding He channel profile probed transversely with 800-nm probe pulses by shearing interferometry at several time delays $0 < \Delta T \leq 6$ ns following the arrival of the channel forming pulse. Abel-inversion analysis of the interferograms reveals channel-expansion dynamics. The initial axial electron density $n_e(r = 0) = 3 \times 10^{19}\,\text{cm}^{-3}$ at $\Delta T \approx 0$, consistent with full ionization, drops to $5 \times 10^{18}\,\text{cm}^{-3}$ by $\Delta T = 3$ ns. At this ΔT, analysis of the profile of the injected 50-mJ, 800-nm pump pulses at the channel exit [see Fig. 1(a), middle row] indicates an optimized TEM_{00} mode with radius $w_0 = 8\ \mu\text{m}$. Since we measure 50% energy throughput (excluding the halo evident in Fig. 1), we infer guided intensity $I_{\text{guided}} = 2 \times 10^{17}\,\text{W/cm}^2$. No distortion of the pump spectrum is observed under this condition [Fig. 1(a), bottom].

Probe pulses ($I_{\text{probe}} \approx 10^{-3} I_{\text{pump}}$) were split from the pump, passed through a variable delay, rotated in polarization by 90°, then recombined with the pump at a thin-film polarizer. An $f/10$ off-axis parabolic mirror focused

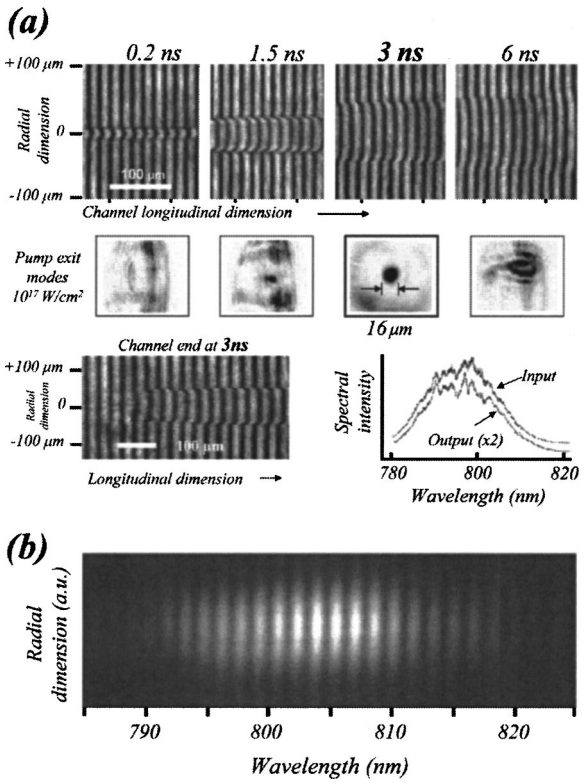

Fig. 1. (a) Characterization of helium plasma channels and guided pump pulses. Top row: transverse Mach–Zehnder interferograms of the expanding channel at four time delays $0.2 \leq \Delta T \leq 6$ ns after the line focus of the channel-forming pulse. Middle row: mode images of the exiting pump pulses, each shown below the corresponding interferograms, for guided intensity $10^{17}\,\text{W/cm}^2$. Bottom row: transverse interferogram of the channel entrance (left) and spatially integrated spectra of the input and output pump pulses at $I_{\text{guided}} = 2 \times 10^{17}\,\text{W/cm}^2$ (right), both at $\Delta T = 3$ ns. (b) Typical frequency-domain interferogram acquired without plasma channel, showing straight fringes obtainable with well-aligned optical system.

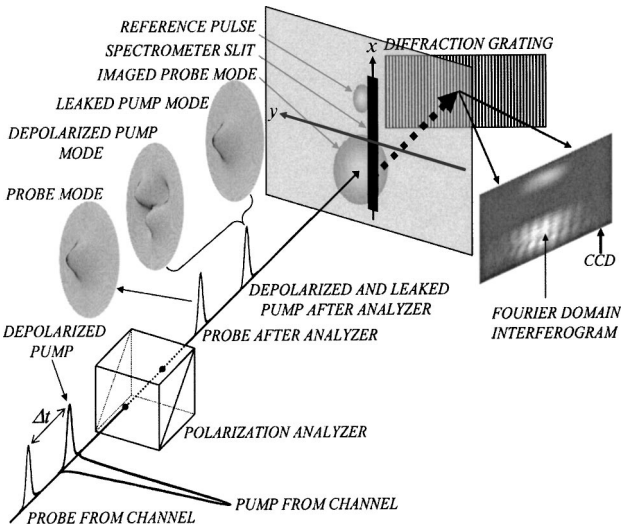

Fig. 2. Schematic of the detection system, showing polarization of the fields E_{pump}, E_{probe}, E_{depol}, and E_{leakage} relative to the spectrometer slit. Transverse mode structure of E_{probe}, E_{depol}, and E_{leakage} is also shown.

the copropagating, orthogonally polarized pump and probe pulses to the channel entrance. A transverse inter-

ferometric image of a typical channel entrance at $\Delta T = 3$ ns is shown in the bottom left corner of Fig. 1(a). The transition region from background to fully formed channel is ~0.25 mm long. Light exiting the channel passed through a high-contrast (extinction ratio $\sim 10^{-6}$) calcite polarization analyzer oriented parallel to the incident probe polarization (hereafter the x direction) and was imaged with 100× magnification onto the entrance slit of a 0.5-m imaging spectrometer oriented along the x direction (see Fig. 2). A charge-coupled device (CCD) detector array recorded single-shot probe (plus pump leakage) spectra with ~1-μm spatial resolution along the x direction, parallel to the slit. Good signal-to-noise ratio required a slit width of ~500 μm, which collected ~1/3 of the FWHM of the imaged mode, and was comparable to shot-to-shot fluctuations in its lateral position. Because of these fluctuations, we were unable to obtain reliable data on the y dependence of the mode structure, since this required translations of the slit between shots. The present results were obtained with the slit located on average slightly off of the imaged mode center, as shown in Fig. 2.

Figure 1(b) shows a test spectrum recorded at $\Delta t = 1.4$ ps with an evacuated chamber and the object plane of the imaging system at the pump–probe focus. The pump field $|E_{\text{leakage}}|$ reaching the detector was intentionally made comparable to $|E_{\text{probe}}|$ by rotating the polarization analyzer. The resulting spectrum is strongly modulated sinusoidally along the λ axis and displays approximately Gaussian intensity variation along the x axis. The modulation disappeared when the pump was blocked, and its period scaled as $(\Delta t)^{-1}$, and therefore results from FDI between the probe and the leaked component E_{leakage} of the pump. The intensity $I(\omega, x)$ recorded on the CCD is proportional to[23]

$$[|E_{\text{leakage}}(\omega)|^2 + |E_{\text{probe}}(\omega)|^2 + 2|E_{\text{leakage}}(\omega)||E_{\text{probe}}(\omega)|\cos(\omega\Delta t)]\exp(-2x^2/w_0^2). \quad (1)$$

As the polarization analyzer was reoriented orthogonally to $\mathbf{E}_{\text{pump}}$, a minimum modulation depth $2|E^{\min}_{\text{leakage}}|/|E_{\text{probe}}| \approx 0.05$, corresponding to minimum leakage $|E^{\min}_{\text{leakage}}|/|E_{\text{pump}}| \approx 0.8 \times 10^{-3}$, could be achieved. This is consistent with the rated intensity discrimination ratio of the calcite polarizer, and with intensity measurements with a photomultiplier tube replacing the spectroscopic system showing pump leakage $< 10^{-6} I_{\text{pump}}$ through the calcite polarizer. With careful matching of k vectors and focal geometries of the pump and probe pulses, flat FDI fringes with no significant tilt or radial structure were achieved, as shown in Fig. 1(b).

3. EXPERIMENTAL RESULTS AND DISCUSSION

A. Frequency-Domain Interferometry in the Plasma Channel for $|\Delta t| \gtrsim 100$ fs

For channeling experiments, the chamber was filled with He gas, a channel was produced, and the object plane of the imaging system was moved to the channel exit. Figure 3 shows single-shot, spatially resolved spectra of $E_{\text{probe}} + E^{\perp}_{\text{pump}}$ at seven pump–probe delays -2 ps $< \Delta t < +1.96$ ps for He channels at $\Delta T = 3$ ns, where $E^{\perp}_{\text{pump}}$ represents the total component of the pump polarized orthogonal to its nominal incident polarization. With the exception of $\Delta t \approx 0$, clear FDI fringes are visible along the λ axis. However, compared with the reference inter-

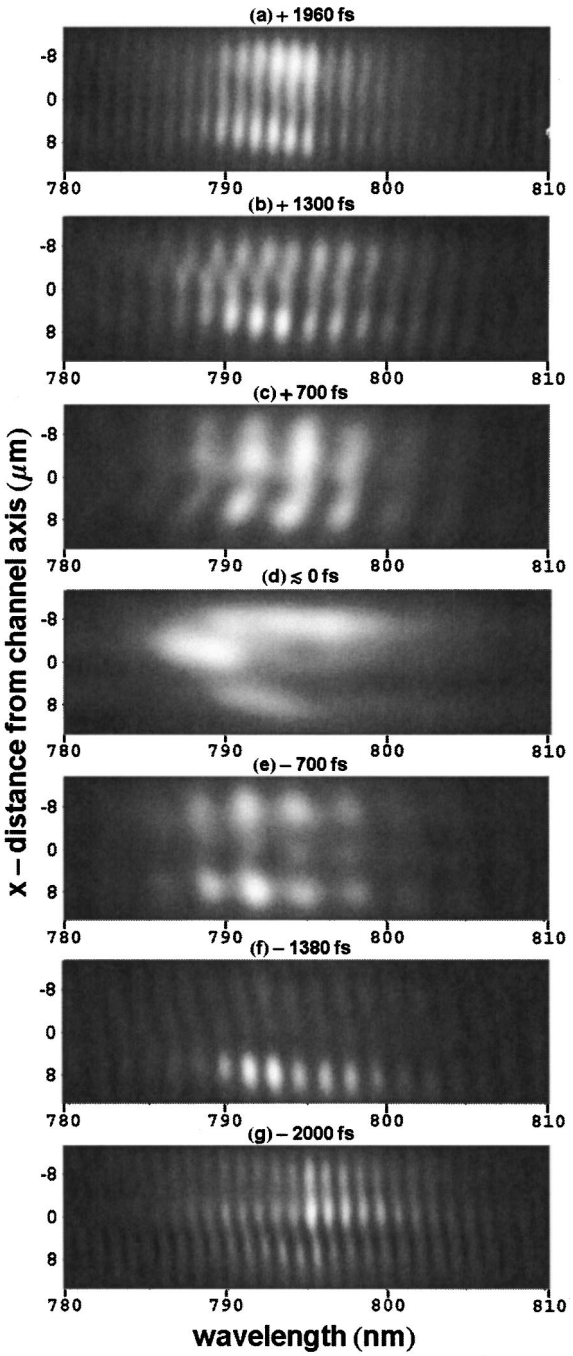

Fig. 3. Single-shot, spatially resolved frequency-domain interferograms from He channel at selected pump–probe time delays from (a) $\Delta t = +2000$ fs to (g) $\Delta t = -2000$ fs. "$\Delta t \lesssim 0$" indicates that peak of probe pulse lies within leading edge of pump pulse. A nonoscillating background has been subtracted off in all cases except $\Delta t \lesssim 0$ to highlight the Δt-dependent fringes along the λ axis. Note fringe tilt that reverses direction as Δt changes sign. For $\Delta t \lesssim 0$, note blueshifted portion of spectrum (785–790 nm) near the channel axis at $x = 0$.

ferograms with $E^{\min}_{\text{leakage}}$, the FDI fringes increased noticeably in amplitude and distorted in spatial structure, demonstrating that an additional field E_{depol}, produced through pump interaction with the channel, contributed to $E^{\perp}_{\text{pump}}$ (i.e., $E^{\perp}_{\text{pump}} = E_{\text{leakage}} + E_{\text{depol}}$). The fields E_{leakage} and E_{depol} are entirely orthogonal to the incident pump. In the cases where fringes are present, a nonoscillating background component has been subtracted from the data in Fig. 3, in order to highlight only the interfering component of period $(\Delta t)^{-1}$.

The interferograms show a distinct tilt in the fringes, indicating an asymmetric x-dependent phase front in $E^{\perp}_{\text{pump}}$. Moreover, the direction of the tilt reverses on going from $\Delta t < 0$ to $\Delta t > 0$ (see corresponding interferograms at $+\Delta t$ and $-\Delta t$ in Fig. 3). This confirms that the fringe tilt originates from the transverse phase structure of $E^{\perp}_{\text{pump}}$, not from an accidental misalignment of $E^{\perp}_{\text{pump}}$ and E_{probe}. Since this feature was not observed in the FDI of two Gaussian pulses (obtained by intentionally rotating the incident pump polarization), we attribute it to the depolarization mechanism. On occasional shots, but without reproducible dependence on Δt, we observed a local minimum on or near the channel axis ($x = 0$), e.g., the $\Delta t = -700$ fs data in Fig. 3. Since the Gaussian probe profile $\exp(-x^2/w_0^2)$ was quite stable from shot to shot, the phase tilt, occasional axial minimum, and other shot-to-shot fluctuations must be attributed to the spatial profile $E_{\text{depol}}(x)$ of depolarized pump light. The intensity $I(\omega, x)$ recorded on the CCD is now proportional to

$$
\begin{aligned}
&|E^{\min}_{\text{leakage}}(\omega)\exp(-x^2/w_0^2) + E_{\text{depol}}(\omega, x)|^2 \\
&\quad + |E_{\text{probe}}(\omega)|^2 \exp(-2x^2/w_0^2) \\
&\quad + 2|E^{\min}_{\text{leakage}}(\omega)\exp(-x^2/w_0^2) \\
&\quad + E_{\text{depol}}(\omega, x)||E_{\text{probe}}(\omega)| \\
&\qquad \times \exp(-x^2/\omega_0^2)\cos[\omega\Delta t + \Delta\phi(x)], \quad (2)
\end{aligned}
$$

where the guided E_{probe}, E_{pump}, and $E^{\min}_{\text{leakage}}$ are Gaussian, and the spatial profile of $E_{\text{depol}}(\omega, x)$ is to be determined from the measurement. $\Delta\phi(x)$ represents a spatially varying phase shift between E_{probe} and $E^{\perp}_{\text{pump}}$. This phase profile could not be measured by blocking the probe and observing only $|E^{\perp}_{\text{pump}}|^2$, i.e., the first term in expression (2). Moreover, the $|E^{\perp}_{\text{pump}}|^2$ signal was too weak even to extract useful single-shot data on its transverse amplitude profile. The homodyne signal $2|E_{\perp}(r, \omega)||E_{\text{probe}}(\omega)|\exp(-r^2/w_0^2)$ characterized this profile more sensitively because, unlike the intensity profile $|E_{\perp}(x)|^2$, it depends linearly on field strength. By using a strong Gaussian E_{leakage} field, the same homodyne technique could be used to characterize the transverse spatial profile of E_{probe}. Such sensitive measurements of the mode structure of E_{probe} and E_{pump} should be important in future experiments documenting their interaction with channeled wakefields and relativistic nonlinearities.

FDI fringe amplitude scaled in proportion to E_{pump} for I_{guided} down to $\sim 3 \times 10^{16}$ W/cm^2. The spatial phase structure of the interferograms also retained the qualitative features described above, suggesting that E_{leakage} and E_{depol} scaled linearly with I_{guided}. Thus nonlinear Kerr rotation of the pump pulse appears not to contribute significantly to depolarization. Linear optical mechanisms, discussed in Section 4, must be responsible.

B. Spectral Probe Blueshifts in the Plasma Channel for $\Delta t \lesssim 0$

At $\Delta t \lesssim 0$, FDI fringes were absent, but we observed blueshifts of the channeled probe spectrum [Figs. 3(d), 4(d)], even though blueshifts were not detected in the transmitted pump [Fig. 1(a), bottom right]. The largest

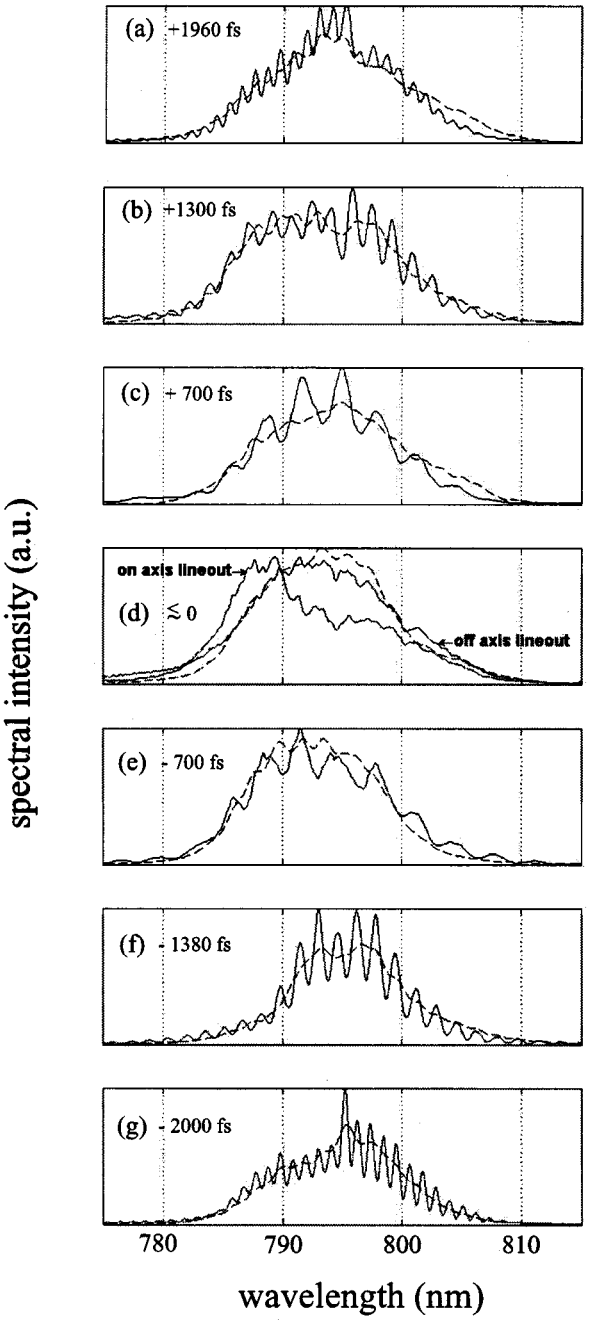

Fig. 4. Lineouts of single-shot interferograms in Fig. 3 without background subtraction (solid curves), compared with spectra of a split-off portion of probe pulse that bypassed the channel (dashed curves). Envelopes of interferogram lineouts coincide closely with reference spectra for $|\Delta t| \gtrsim 50$ fs [(a)–(c) and (e)–(g)]. At $\Delta t \lesssim 0$ [panel (d)], a blueshift of $\Delta\lambda \sim 5$ nm is evident in the on-axis lineout of the channeled probe.

blueshift ($\Delta\lambda_{\text{probe}} \sim 5 \pm 1$ nm) was observed with the probe in the leading edge of the pump ($-50 < \Delta t < 0$ fs). The optimum Δt fluctuated somewhat from shot to shot, because of pump intensity and channel fluctuations. Thus we labeled Figs. 3(d) and 4(d) "$\Delta t \lesssim 0$". The dependence of the blueshifts on Δt identifies them as shifts in E_{probe}, because shifts in E_{depol} would not depend on Δt. The spatial dependence of the shift evident in Figs. 3(d) and 4(d) corroborates this conclusion. The blueshifted portion of the detected spectrum (785–790 nm) is invariably concentrated on the channel axis [$x = 0$ in Fig. 3(d) and on-axis lineout in Fig. 4(d)], where E_{probe} and E_{pump} are maximum.

In order to quantify the blueshift, transmitted probe spectra were compared with spectra of reference pulses split from the same pulse that bypassed the channel. Figure 4 superposes lineouts (at fixed x and several Δt) of corresponding probe and reference spectra. Here, the nonoscillating background has not been subtracted off from the interferograms at $|\Delta t| > 100$ fs, thus clearly showing the relative amplitude $2|E_{\text{depol}}|/|E_{\text{probe}}| \approx 0.1$ of FDI fringes and probe intensity. Reference and probe spectra were normalized to yield equivalent integrated energy, ensuring valid comparison. The envelopes of the interferograms at $|\Delta t| > 100$ fs fit the envelope of the reference spectrum very closely in all cases.

The prominent $\Delta t \lesssim 0$ blueshift signifies ionization by the leading edge of the pump of residual gas left incompletely ionized after channel formation. Ionization fronts for both He ionization stages indeed occur in the leading edge of the pump pulse, because their threshold intensities ($\sim 10^{15}$ and 10^{16} W/cm^2 for He^+ and He^{2+}, respectively)[24] are less than I_{guided}. They can be reconciled with absence of a detectable pump blueshift because a leading edge ionization front would shift a relatively small fraction of the pump energy, whereas the peak of the probe pulse can "ride" the ionization front, thereby causing most of its energy to shift. Thus the blueshift of an appropriately timed probe pulse more sensitively characterizes residual ionization than the transmitted pump spectrum [Fig. 1(a), bottom right] alone.

This measurement by itself does not pinpoint the location of the residual incompletely ionized gas. The greatest concentration is expected near the channel entrance and exit, where ionization by the channel-forming pulse is inefficient. Here the entering (exiting) pulse interacts with incompletely ionized gas at approximately full I_{guided} over path length $z \sim z_R \sim 250\,\mu$m. On the other hand, once coupled into the channel, the pulse interacts with the plasma over path length $z \sim 60 z_R$. Thus, since the probe blueshift[10]

$$\Delta\lambda_{\text{probe}} \approx z\lambda_{\text{probe}}^3 \frac{r_e}{2\pi c} \frac{\mathrm{d}n_e}{\mathrm{d}t} \tag{3}$$

is proportional to z (r_e is the classical electron radius), ionization of residual gas $\sim 60\times$ less dense than in the entrance (exit) region could cause an equivalent blueshift. To distinguish these possibilities, one could systematically shorten the channel by masking the channel-generating pulse incident on the axicon. However, this alters the structure of the entrance and/or exit of the channel in uncontrolled ways. Thus, as a cleaner test, we repeated the experiment with a frequency-doubled probe pulse in a channel identical to that used to measure the blueshift of the 800-nm probe (length 1.5 cm, axial density $n_e < 0.7 \pm 0.2 \times 10^{10}$ cm^{-3} from transverse interferometry). The 400-nm probe walks off from the pump by approximately a pulse duration ($\tau_p = 80$ fs) because of group-velocity mismatch. Since the pump-induced ionization front is less than τ_p, any contribution to $\Delta\lambda_{\text{probe}}^{400\text{ nm}}$ from the 1.5-cm channel transit should be substantially reduced. The measured blueshifts of the 400-nm probe are shown in Fig. 5. Blueshifts $\Delta\lambda_{\text{probe}}^{400\text{ nm}} \approx 0.8 \pm 0.2$ nm are observed at $\Delta t \lesssim 0$. Within measurement error, these shifts are consistent with those observed with the 800-nm probe, scaled by the factor λ_{probe}^3. We must conclude that the 800- and 400-nm probes interact with the pump-induced ionization front over roughly equal path lengths that are shorter than the channel length L_{ch}, suggesting that the channel itself contributes relatively little to the observed blueshift. This not only confirms previous conclusions about full ionization within the He channel,[7] but provides a much more stringent test than diagnostics based on the guided pump pulse or transverse channel interferometry.

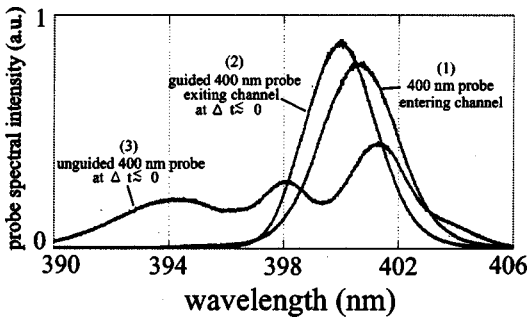

Fig. 5. Spatially averaged, time-resolved single-shot spectra of 400-nm probe pulses under three conditions: (1) entering the channel; (2) exiting the channel following injection at $\Delta t \lesssim 0$ behind the pump pulse; (3) after copropagating with pump at $\Delta t \lesssim 0$ through 700-Torr He gas without channel. Spectra of 400-nm probe pulses exiting the channel at $|\Delta t| \gtrsim 100$ fs were indistinguishable from those of the entering pulses.

From expression (2), the observed $\Delta t \lesssim 0$ shifts are consistent with ionizing average $\Delta n_e \sim 10^{18}$ cm^{-3} over interaction length $z_R \approx 250\,\mu$m, the approximate length of the channel entrance region [see Fig. 1(a), bottom left], assuming $\Delta t \approx -40$ fs (half a pulse duration). This is $\sim 60\times$ less than Δn_e from fully ionizing the He backfill gas. Indeed, we observe $5\times$ to $10\times$ larger $\Delta\lambda_{\text{probe}}$ from the backfill He gas as illustrated by the $\Delta\lambda_{\text{probe}}^{400\text{ nm}}$ data for the unguided 400-nm probe in Fig. 5. The ratio is <60 because the latter shifts, unlike the former, were accompanied by severe defocusing, which shortens the effective interaction length. Taken together, the $\Delta t \lesssim 0$ blueshifts of 800-nm and 400-nm probe pulses yield a complete diagnostic of residual unionized gas in the plasma channel.

4. ANALYSIS OF PUMP DEPOLARIZATION

Intensity-*independent* polarization rotation can occur cumulatively during propagation through the $\sim$1-cm-long

main plasma channel, analogous to depolarization mechanisms in single-mode glass fibers[25] that result in hybrid modes with mixed polarization.[26] This effect can be enhanced locally near the entrance and exit, where the channel typically is denser and narrower than in the central portion. We analyze each of these possibilities in turn. The main observations to explain are (1) depolarization amplitude $|E_{\mathrm{depol}}/E_{\mathrm{pump}}|_{\max} \approx 10^{-3}$, determined from the observed ratio $2|E_{\mathrm{depol}}|/|E_{\mathrm{probe}}| \approx 10^{-1}$ of FD fringe amplitude to probe intensity and the probe/pump intensity ratio $|E_{\mathrm{probe}}/E_{\mathrm{pump}}|^2 \approx 10^{-3}$; (2) the tilted FD fringes, indicating a phase shift of E_{depol} on crossing the channel axis.

A. Amplitude and Spatial Profile of Depolarized Light

Propagation within the fully ionized channel is governed by the Maxwell equations $\nabla\times\mathbf{E} = i\omega/c\mathbf{B}$ and $\nabla\times\mathbf{B} = -i\epsilon\omega/c\mathbf{E}$, which can be combined to yield an equation for $\mathbf{B}$:

$$\nabla \times \left(\frac{1}{\epsilon}\nabla\times\mathbf{B}\right) = \frac{\omega^2}{c^2}\mathbf{B}, \tag{4}$$

where $\epsilon = 1 - \omega_p^2/\omega^2$ is the dielectric permittivity of the plasma channel with transverse density profile $\omega_p^2(r)$. If we write $\mathbf{B} = \boldsymbol{\mathcal{B}}\exp(ik_0 z)$, introducing the carrier wave number $k_0^2 = (\omega^2 - \omega_{p0}^2)/c^2$ on the channel axis ($r = 0$), where $\omega_p^2 = \omega_{p0}^2$, Eq. (4) simplifies to

$$-2ik_0\frac{\partial\boldsymbol{\mathcal{B}}}{\partial z} = \left(\nabla_\perp^2 - \frac{\omega_p^2 - \omega_{p0}^2}{c^2}\right)\boldsymbol{\mathcal{B}} + \frac{1}{\epsilon}\nabla\epsilon\times[\nabla\times\boldsymbol{\mathcal{B}}]. \tag{5}$$

The second term on the right-hand side is responsible for depolarizing the field to create hybrid modes. For the idealized case of a cylindrically symmetric channel in which density $\omega_p^2 = \omega_{p0}^2(1 + r^2/r_{\mathrm{ch}}^2)$ varies parabolically with radius ($r_{\mathrm{ch}} \approx 33\,\mu$m at $\Delta T = 3$ ns), Eq. (5) becomes

$$-2ik_0\frac{\partial\boldsymbol{\mathcal{B}}}{\partial z} = \left(\nabla_\perp^2 - \frac{\omega_{p0}^2 r^2}{c^2 r_{\mathrm{ch}}^2}\right)\boldsymbol{\mathcal{B}} - \frac{2\omega_{p0}^2}{\omega^2 r_{\mathrm{ch}}^2}\left(\frac{\partial\mathcal{B}_x}{\partial y} - \frac{\partial\mathcal{B}_y}{\partial x}\right) \times (x\hat{y} - y\hat{x}), \tag{6}$$

where we have assumed $\epsilon \approx 1$ (but retained its derivatives) and neglected the small $\mathcal{B}_z$ component. The second term on the right-hand side of Eq. (6) now explicitly couples $\mathcal{B}_x$ and $\mathcal{B}_y$. Thus a linearly polarized wave injected with $\boldsymbol{\mathcal{B}} = \mathcal{B}_x\hat{x}$ develops a small $\mathcal{B}_y$ component as it propagates. Assuming $\mathcal{B}_y \ll \mathcal{B}_x$, Eq. (6) can be solved perturbatively. The unperturbed $\mathcal{B}_x$ is the analytic solution of Eq. (6) without the coupling term. In the main channel, this is given by $\mathcal{B}_x = \mathcal{B}_0\exp(-r^2/2\sigma^2) \times \exp(-i\Delta kz)$, where $\sigma = (cr_{\mathrm{ch}}/\omega_{p0})^{1/2} \approx 9.5\,\mu$m is the constant e^{-1} radius of the guided intensity profile and $\Delta k = \omega_{p0}/k_0 c r_{\mathrm{ch}} \approx 15\,\mathrm{cm}^{-1}$ is the change in $k_0 \approx 7.9 \times 10^4\,\mathrm{cm}^{-1}$ for the guided mode. The perturbation $\mathcal{B}_y$ is then the solution of

$$-2ik_0\frac{\partial\mathcal{B}_y}{\partial z} = \left(\nabla_\perp^2 - \frac{\omega_{p0}^2 r^2}{c^2 r_{\mathrm{ch}}^2}\right)\mathcal{B}_y + \mathcal{B}_0\frac{\omega_{p0}^2}{\omega^2 r_{\mathrm{ch}}^2}\frac{2xy}{\sigma^2} \times \exp[-(x^2 + y^2)/2\sigma^2]\exp(-i\Delta kz), \tag{7}$$

which can be written as the sum of driven and homogeneous solutions

$$\mathcal{B}_y(x, y, z) = \mathcal{B}_0\frac{\omega_{p0}^2}{2\omega^2}\frac{xy}{r_{\mathrm{ch}}^2}\exp[-(x^2 + y^2)/2\sigma^2] \times \exp(-i\Delta kz)\{1 - \exp[-i(\Delta k_1 - \Delta k)z]\}, \tag{8}$$

where $\Delta k_1 = 3\omega_{p0}/k_0 c r_{\mathrm{ch}} = 3\Delta k$ and the channel was assumed to start abruptly at $z = 0$ with $\mathcal{B}_y(z = 0) = 0$ as an initial condition. The term in curly brackets arises from the slightly different phase velocities of the driving pulse and depolarized component. Because of this term, the amplitude of $\mathcal{B}_y$ does not grow monotonically with z, but fluctuates with period $(\Delta k_1 - \Delta k)^{-1} \sim 0.04$ cm that, for our experimental parameters, is much shorter than L_{ch}.

Equation (8) predicts field amplitude ratio $|\mathcal{B}_y/\mathcal{B}_0|$, which can be compared with the measured $|E_{\mathrm{depol}}/E_{\mathrm{pump}}|$ at any spatial position. It also predicts a transverse mode structure of the form $xy\exp[-(x^2 + y^2)]$ in $\mathcal{B}_y$ and thus in the corresponding electric field component $\mathbf{E}_{\mathrm{depol}}(x, y) \sim \nabla\times\boldsymbol{\mathcal{B}}_y$. For comparison with the measurements in Subsection 2A, we must consider the total field $E_{\mathrm{pump}}^{\perp} = E_{\mathrm{depol}}(x) + E_{\mathrm{leakage}}^{\min}(x) = (|E_{\mathrm{depol}}|\exp(i\Phi)xy + |E_{\mathrm{leakage}}^{\min}|)\exp[-(x^2 + y^2)/2\sigma^2]$, where Φ represents an x-independent phase shift of E_{depol} relative to $E_{\mathrm{leakage}}^{\min}$ arising from the term $\{1 - \exp[-i(\Delta k_1 z - \Delta k)z]\}$. The spectrometer sampled the imaged exit mode along x using a slit of width Δy around a fixed nonzero value of y. Thus $E_{\mathrm{depol}}(x) \propto x$. The phasor diagram in Fig. 6 depicts an example of the addition of $E_{\mathrm{depol}}(x)$ to E_{leakage} at three positions ($x = \pm x_0, 0$) for the case $E_{\mathrm{depol}}(x_0) \approx E_{\mathrm{leakage}}$ and $\Phi \approx \pi/4$. This example shows how the phase $\Delta\phi(x)$ of the resultant field $E_{\mathrm{pump}}^{\perp}$ varies continuously between $+x_0$ and $-x_0$, qualitatively consistent with the observed tilt in the FDI fringes. Quantitative details of the fringe pattern depend on the relative amplitudes of E_{depol}, E_{leakage}, and E_{probe}, which can be estimated from the observations, and on Φ, which must be treated as an adjustable parameter. We were unable to confirm reliably the prediction of Eq. (8) that $\mathcal{B}_y$ should vanish for a narrow slit at $y = 0$ (in which case E_{depol} would not contribute to the FDI fringes) because of the finite slit width and shot-to-shot fluctuations ($\delta y \sim \sigma$) in the lateral position of the imaged mode.

B. Depolarization within the Main Channel

If we substitute the parameters ($\omega_{p0} \approx 10^{14}\,\mathrm{s}^{-1}$, $r_{\mathrm{ch}} \approx 30\,\mu$m) of the main channel, Eq. (8) predicts $|\mathcal{B}_y/\mathcal{B}_0|_{\max} = (\omega_{p0}/\omega)^2(\sigma/r_{\mathrm{ch}})^2 \approx 10^{-4}$, taking $|1 - \exp[-i \times (\Delta k_1 z - \Delta k)z] \sim 1$ and replacing $xy\exp[-(x^2 + y^2)/2\sigma^2]$ with its maximum value $2\sigma^2$. This is more than one order of magnitude smaller than the observed

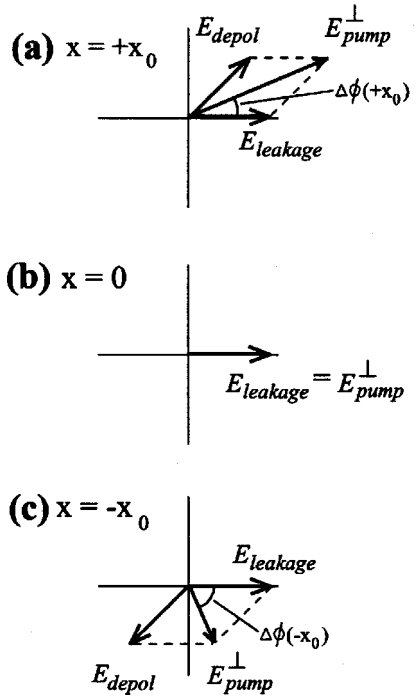

Fig. 6. Phasor diagrams depicting the effect of adding the copolarized fields $E_{\mathrm{depol}}(x) = |E_{\mathrm{depol}}|\exp(i\Phi)x\exp(-x^2)$ and E_{leakage} (taken as a pure real quantity) on the phase $\Delta\phi(x)$ of the resultant field $E^{\perp}_{\mathrm{pump}}(x)$ at three transverse spatial positions: (a) $x = +x_0$, (b) $x = 0$, and (c) $x = -x_0$. The horizontal and vertical axes denote the real and imaginary components, respectively, of each field. For the example shown, there is an x equals independent phase difference $\Phi \approx \pi/4$ between E_{depol} and E_{leakage}.

$|E_{\mathrm{depol}}/E_{\mathrm{pump}}|_{\max}$. Thus a cylindrically symmetric channel with these parameters cannot produce the observed depolarized pump light.

We considered the possibility that deviations from cylindrical symmetry within the main channel might contribute to rotation of the pump polarization. For example, a pump pulse polarized along the direction $\mathbf{e}_0 = \hat{x}\cos\theta + \hat{y}\sin\theta$ experiences polarization rotation in an elliptic channel of biparabolic shape $\omega_p^2 = \omega_{p0}^2(1 + x^2/\rho_x^2 + y^2/\rho_y^2)$, because the propagation wave numbers k_x and k_y for the x- and y-polarized components differ. In this case, the dominant effect is the polarization rotation of the lowest-order Gaussian mode $\mathcal{B}_{x,y} = \mathcal{B}_0\exp(-x^2/2\sigma_x^2) \times \exp(-y^2/2\sigma_y^2)\exp(-i\Delta kz)$, if injected with $\theta \neq n\pi/2$. However, we observed nearly circular Gaussian modes exiting the channel, so it is unlikely that ρ_x and ρ_y differ by more than ~10%. By extending the previous analysis [Eqs. (4)–(8)] to this case, we found that, even for the case $\theta = \pi/4$ of maximum polarization rotation, depolarization amplitude $E_{\mathrm{depol}}/E_{\mathrm{pump}}$ of only 10^{-4} is expected after $L_{\mathrm{ch}} = 1$ cm, also well short of the observed depolarization amplitude. Moreover, this rotated lowest-order mode lacks the observed asymmetric transverse phase structure. We conclude that depolarization mechanisms within the main channel cannot explain the observed effect.

C. Depolarization at the Channel Entrance and Exit

Because of the short coherence length $(\Delta k_1 - \Delta k)^{-1} \sim 400\ \mu$m of the depolarization mechanism described by Eqs. (4)–(8), short transitional regions near the entrance and exit of the channel can dominate the depolarization process. In these regions, the channel remains incompletely formed at the time of injection. Thus the local radius r'_{ch} is less than the radius r_{ch} of the main channel by factor of ~2–3 over a distance of a few hundred microns, as seen in the bottom left interferogram in Fig. 1(a). In addition, assuming the gas is fully ionized, the local axial plasma density $(\omega'_{p0})^2$ is higher than in the main channel by a similar factor, because the central density minimum has not fully formed. Even if the channel-forming pulse does not completely ionize the gas in these regions, the leading edge of the entering pump pulse will complete the ionization, thus ensuring $\omega'_{p0} > \omega_{p0}$ at its peak.

To estimate the resulting depolarization, we model the entrance and exit regions of the main channel as short cylindrically symmetric channels of radius r'_{ch}, axial density ω'_{p0}, and length $L'_{\mathrm{ch}} \lesssim (\Delta k_1 - \Delta k)^{-1}$, into which a lowest-order Gaussian mode with radius $\sigma = (cr_{\mathrm{ch}}/\omega_{p0})^{1/2}$ of the stably propagating eigenmode of the *main* channel is injected. Although σ exceeds the stably guided radius $\sigma' = (cr'_{\mathrm{ch}}/\omega'_{p0})^{1/2}$ of the entrance/exit channels, the resulting tendency to focus can be neglected because L'_{ch} is very short. We thus assume σ remains approximately constant in the auxiliary end channels. The depolarized mode emerging from one of them is then given by Eq. (8) with $\omega_{p0} \to \omega'_{p0}$ and $r_{\mathrm{ch}} \to r'_{\mathrm{ch}}$. Approximating $|\exp(-i\Delta kz) - \exp(-i\Delta k_1 z)| \sim 1$ and using $|xy\exp[-(x^2 + y^2)/2\sigma^2]|_{\max} = 2\sigma^2$ as before, we get a maximum polarization ratio

$$|\mathcal{B}'_y/\mathcal{B}_0|_{\max} = (\omega'_{p0}/\omega)^2(\sigma/r'_{\mathrm{ch}})^2. \tag{9}$$

This ratio is larger than the estimate for the main channel by a factor $(\omega'_{p0}/\omega_{p0})^2(r_{\mathrm{ch}}/r'_{\mathrm{ch}})^2$. For example, the physically reasonable numbers $r'_{\mathrm{ch}} \approx r_{\mathrm{ch}}/2$ and $(\omega'_{p0}/\omega_{p0})^2 \approx 3$ yield $|\mathcal{B}'_y/\mathcal{B}_0|_{\max} \approx 10^{-3}$, very close to the observed ratio $|E_{\mathrm{depol}}/E_{\mathrm{pump}}|_{\max}$. This explanation is also consistent qualitatively with the observed radial structure of $E_{\mathrm{depol}}(x, y)$.

Figure 7 presents calculated FD interferograms for the same Δt used for the measurements in Fig. 3. The calculations were made by evaluating the third term in Eq. (2) with $E_{\mathrm{depol}}(\omega, x)$ given a transverse structure $|E_{\mathrm{depol}}|\exp(i\Phi)x\exp(-x^2)$ based on Eq. (8), and amplitude $|E_{\mathrm{depol}}| = |E^{\min}_{\mathrm{leakage}}| \approx 10^{-3}E_{\mathrm{pump}}$ based on the arguments in the previous paragraph. For the calculations in Fig. 7, we used $\Phi = \pi/4$. The calculations qualitatively reproduce the observed tilt of the fringes, including the reversal with sign of Δt. Moreover, this general fringe structure is not highly sensitive to a particular choice of the ratio $|E_{\mathrm{depol}}|/|E^{\min}_{\mathrm{leakage}}|$ or the phase factor Φ, although variations in these parameters do affect some details of the calculated interferograms. The most severe alteration occurs for $\Phi \approx 0$ or π, for which the fringe tilt disappears. However, this appears to be a special case that is rarely observed. Other choices of Φ preserve the overall tilted fringe structure shown in Fig. 7 but introduce curvature and/or discontinuous kinks into the fringes similar to those evident in Figs. 3(b) and 3(g). Such variations in Φ would indeed be expected from shot-to-shot variations in the length and structure of the auxiliary end channel. When $|E_{\mathrm{depol}}|$ becomes significantly

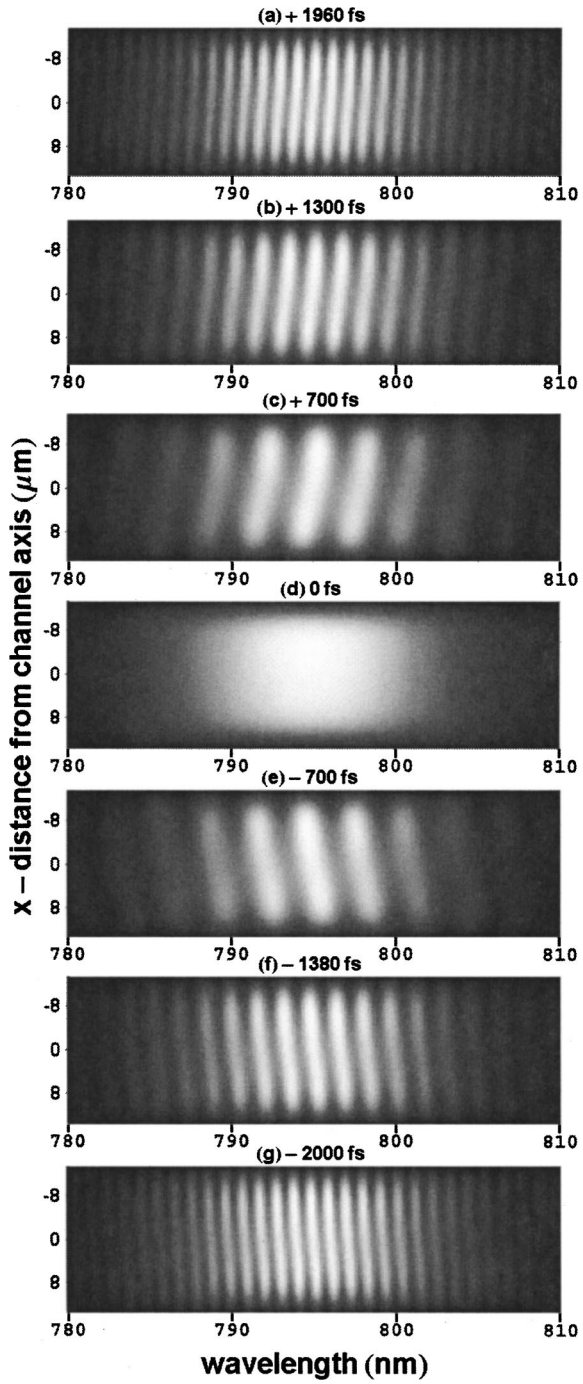

Fig. 7. Model of FD interferograms produced by interference of Gaussian guided probe pulse with depolarized pump light produced in a ~300-μm entrance region of the channel.

larger than $|E_{\text{leakage}}^{\min}|$, an axial minimum develops in the calculated interferogram. This is because the transverse amplitude is dominated by $|E_{\text{depol}}| \propto x$, which vanishes on axis. Laser shots that produce large $|E_{\text{depol}}|$, perhaps because of an unusually dense or narrow entrance region, may explain the occasional observation of an axial minimum in the interferogram.

Since the pump depolarization and ionization blueshifting effects appear to originate near the channel ends, they should provide effective diagnostics of strategies to manipulate the structure of the channel ends. For example, auxiliary laser pulses have been used to preionize the plasma[8] or to generate a short length of strongly heated plasma near the end of the line focus to open a "funnel" to improve coupling.[27] The latter technique has been shown to suppress the "halo" often observed around the guided pump mode [see, e.g., 3-ns mode in Fig. 1(a)], suggesting that this halo may be closely correlated with the depolarization and blueshifting effects reported here.

5. CONCLUSION

We have implemented pump–probe measurements in ~1-cm-long preformed plasma channels to characterize pump depolarization and ionization blueshifting more sensitively than is possible through measurements of the pump pulse alone. The use of pump and probe pulses of the same wavelength (800 nm) yields two advantages over traditional two-color pump–probe experiments: first, it permits a simplified form of frequency-domain interferometry by employing only a single probe pulse that interferes with a component of the pump (provided $\Delta t \gtrsim \pi/\Delta\omega$), and second, it ensures group-velocity matching throughout channel transit. In future experiments, we expect to use this form of phase-sensitive FDI to measure these modulations with sensitivity of $\Delta n/n \sim 10^{-4}$ or better.

In addition to serving as a method to isolate the probe light from scattered pump light at the detector, the use of an orthogonally polarized probe in the interferometry also enables sensitive homodyne-characterization of the weak, depolarized component of the hybrid pump mode that would otherwise be swamped by the main portion of the pump. We have used this method to show that the depolarized component of a guided hybrid Gaussian pump pulse has a strongly non-Gaussian mode structure and weak blueshift that fluctuate from shot to shot. In future experiments, the same technique can be used in reverse to measure non-Gaussian spatial structure induced on the probe (e.g., by pump-induced wakefields) by FDI with a Gaussian pump leakage field of adjustable amplitude. The present results show that, in such measurements, the intentionally rotated component E_{leakage} of the pump field should significantly exceed the depolarized component $E_{\text{depol}} \sim 10^{-3} E_{\text{pump}}$, so that a well-characterized Gaussian reference pulse interferes with the probe. Even so, the structure of E_{depol} determined here may have to be taken into account in interpreting finer details of such measurements.

Comparative measurements with probes of different wavelength yields information about the longitudinal location of the index modulations to be determined, and we have shown that observed probe ionization blueshifts cannot originate inside the plasma channel. These observations, together with supporting models, suggest that both the depolarization and blueshifting occur primarily at the channel entrance.

ACKNOWLEDGMENTS

This research was supported primarily by U.S. Department of Energy grant DEFG03-96-ER-40954, with additional support from the National Science Foundation

FOCUS Center grant PHY-0114336 and Office of Naval Research grant N00014-03-1-0639.

REFERENCES

1. P. Sprangle and B. Hafizi, "Guiding and stability of short laser pulses in partially stripped ionizing plasmas," Phys. Plasmas **6**, 1683–1689 (1999), and references therein.
2. Y. Ehrlich, C. Cohen, A. Zigler, J. Krall, P. Sprangle, and E. Esarey, "Guiding of high-intensity laser pulses in straight and curved plasma channel experiments," Phys. Rev. Lett. **77**, 4186–4189 (1996).
3. D. Kaganovich, P. Sasorov, C. Cohen, and A. Zigler, "Variable profile capillary discharge for improved phase matching in a laser wakefield accelerator," Appl. Phys. Lett. **75**, 772–774 (1999).
4. T. Hosokai, M. Kando, H. Dewa, H. Kotaki, S. Kondo, N. Hasegawa, K. Nakajima, and K. Horioka, "Optical guidance of terawatt laser pulses by the implosion phase of a fast Z-pinch discharge in a gas-filled capillary," Opt. Lett. **25**, 10–12 (2000).
5. A. Butler, D. J. Spence, and S. M. Hooker, "Guiding of high-intensity laser pulses with a hydrogen-filled capillary discharge waveguide," Phys. Rev. Lett. **89**, 185003 (2002).
6. C. G. Durfee III, J. Lynch, and H. M. Milchberg, "Development of a plasma waveguide for high-intensity laser pulses," Phys. Rev. E **51**, 2368–2389 (1995).
7. E. W. Gaul, S. P. Le Blanc, A. R. Rundquist, R. Zgadzaj, H. Langhoff, and M. C. Downer, "Production and characterization of a fully ionized He plasma channel," Appl. Phys. Lett. **77**, 4112–4114 (2000).
8. P. Volfbeyn, E. Esarey, and W. P. Leemans, "Guiding of laser pulses in plasma channels created by the ignitor-heater technique," Phys. Plasmas **6**, 2269–2277 (1999).
9. S. P. Nikitin, I. Alexeev, J. Fan, and H. M. Milchberg, "High efficiency coupling and guiding of intense femtosecond laser pulses in preformed plasma channels in an elongated gas jet," Phys. Rev. E **59**, R3839–R3842 (1999).
10. W. M. Wood, C. W. Siders, and M. C. Downer, "Measurement of femtosecond ionization dynamics of atmospheric density gases by spectral blueshifting," Phys. Rev. Lett. **67**, 3523–3526 (1991).
11. P. Blanc, P. Audebert, F. Fallies, J. P. Geindre, J. C. Gauthier, A. Dos Santos, A. Mysyrowicz, and A. Antonetti, "Phase dynamics of reflected probe pulses from sub-100-fs laser-produced plasmas," J. Opt. Soc. Am. B **13**, 118–124 (1996).
12. M. K. Grimes, A. R. Rundquist, Y.-S. Lee, and M. C. Downer, "Experimental identification of vacuum heating at femtosecond-laser-irradiated metal surfaces," Phys. Rev. Lett. **82**, 4010–4013 (1999).
13. K. Y. Kim, I. Alexeev, E. Parra, and H. M. Milchberg, "Time-resolved explosion of intense-laser-heated clusters," Phys. Rev. Lett. **90**, 023401 (2003).
14. C. W. Siders, S. P. Le Blanc, D. Fisher, T. Tajima, M. C. Downer, A. Babine, A. Stepanov, and A. Sergeev, "Laser wakefield excitation and measurement by femtosecond longitudinal interferometry," Phys. Rev. Lett. **76**, 3570–3573 (1996).
15. J. R. Marques, R. Dorchies, F. Amiranoff, P. Audebert, J. C. Gauthier, J. P. Geindre, A. Antonetti, T. M. Antonsen, P. Chessa, and P. Mora, "Laser wakefield: experimental study of nonlinear radial electron oscillations," Phys. Plasmas **5**, 1162–1177 (1998).
16. S. P. Le Blanc, M. C. Downer, R. Wagner, S.-Y. Chen, A. Maksimchuk, G. Mourou, and D. Umstadter, "Temporal characterization of a self-modulated laser wakefield," Phys. Rev. Lett. **77**, 5381–5384 (1996).
17. A. Ting, K. Krushelnick, C. I. Moore, H. R. Burris, E. Esarey, J. Krall, and P. Sprangle, "Temporal evolution of self-modulated laser wakefields measured by coherent Thomson scattering," Phys. Rev. Lett. **77**, 5377–5380 (1996).
18. H. Kotaki, M. Kando, T. Oketa, S. Masuda, J. K. Koga, S. Kondo, S. Kanazawa, T. Yokoyama, T. Matoba, and K. Nakajima, "Direct measurement of coherent ultrahigh wakefields excited by intense ultrashort laser pulses in a gas-jet plasma," Phys. Plasmas **9**, 1392–1400 (2002).
19. S. P. Le Blanc, E. W. Gaul, N. M. Matlis, A. R. Rundquist, and M. C. Downer, "Single-shot measurement of temporal phase shifts by frequency-domain holography," Opt. Lett. **25**, 764–766 (2000).
20. K. Y. Kim, I. Alexeev, and H. M. Milchberg, "Single-shot supercontinuum spectral interferometry," Appl. Phys. Lett. **81**, 4124–4126 (2002).
21. S. C. Wilks, J. M. Dawson, W. B. Mori, T. Katsouleas, and M. E. Jones, "Photon accelerator," Phys. Rev. Lett. **62**, 2600–2603 (1989).
22. J. M. Dias, L. Oliveira e Silva, and J. T. Mendonca, "Photon accelerator and interferometry diagnostics of laser wakefields," in *Proceedings of the 1st JAERI-Kansai International Workshop on Ultrashort-Pulse Ultrahigh-Power Lasers and Simulation for Laser–Plasma Interactions* (Japan Atomic Energy Research Institute, Tokai, 1997), pp. 1–24.
23. L. Lepetit, G. Cheriaux, and M. Joffre, "Linear techniques of phase measurement by femtosecond spectral interferometry for applications in spectroscopy," J. Opt. Soc. Am. B **12**, 2467–2474 (1995).
24. S. Augst, D. Strickland, D. D. Meyerhofer, S. L. Chin, and J. H. Eberly, "Tunneling ionization of noble gases in a high-intensity laser field," Phys. Rev. Lett. **63**, 2212 (1989).
25. W. K. Burns, Robert P. Moeller, and Chin-lin Chen, "Depolarization in a single-mode optical fiber," J. Lightwave Technol. **LT-1**, 44–49 (1983).
26. A. W. Snyder and J. D. Love, *Optical Waveguide Theory* (Kluwer Academic, Dordrecht, The Netherlands, 1983).
27. K. Y. Kim, I. Alexeev, J. Fan, E. Parra, and H. M. Milchberg, "Plasma waveguides: addition of end funnels and generation in clustered gases," in *Advanced Accelerator Concepts, Tenth Workshop*, C. E. Clayton and P. Muggli, eds. (American Institute of Physics, Melville, N.Y., 2002), pp. 646–653.